

Dye Degradation Comparison Studies of Methylene Blue and Methyl Orange by Synthesized Zn Doped Fibrous Wollastonite.

M ABHIJIT* and B. V SURESH KUMAR

Dos in Earth Science, Manasagangothri, University of Mysore, Mysuru.

Abstract

In this study, Zn-doped calcium silicate (Zn-WO) materials were successfully synthesized. As precursors, $\text{Ca}(\text{OH})_2$, SiO_2 , and ZnO were utilized, then the hydrothermal experiment was conducted for 6 hours at 1050°C . In this work, the behavior of two groups of raw materials exposed to isobaric and same temperature circumstances is described. The synthesized sample was examined using XRD, SEM, EDAX, BET, and UV-Vis spectroscopic techniques to understand the adsorbent's physicochemical characteristics, and the adsorbent's performance was evaluated. The energy band gap of 2.70 eV and 2.62 eV with the surface area calculated by BET of $92.4\text{ m}^2/\text{g}$ and $112.6\text{ m}^2/\text{g}$ for Zn-WO-1 and Zn-WO-2 respectively were found in this research. After 150 minutes of Zn-WO-1 and Zn-WO-2, the maximum amount of degradation by absorption under dark and sunlight photocatalytic activity compared with the two synthesized samples, 88.4% and 92.3% of methylene blue and 80.9% and 85.3% of methyl orange, took place.



Article History

Received: 21 December 2022

Accepted: 25 January 2023

Keywords

Hydrothermal;
Methylene blue;
Methyl orange;
Wollastonite.

Introduction


Aquatic pollution, in one form or another, is one of the greatest warning threats to our ecosystem. In comparison to pollutants like metal ions, dyes, and sprays of insecticide, dye pollution causes the most harm to the ecosystem.¹ It has also been reported in a scathing review of textile wastewater.² Because of its benefits, including high efficacy, cheap cost, simplicity of design, and non-generation of harmful compounds, the adsorption process has been used successfully to remove pollutants among the many

removal procedures.^{3,4,5} Under UV light irradiation, the nanostructured semiconductors may effectively destroy a variety of organic contaminants.⁶ The quick recombination of photogenerated electrons and holes results in a low quantum yield, which makes it extremely difficult to increase the photocatalytic activity of semiconductors to satisfy the needs of workable applications.⁷ To assess the metal oxide catalytic activity of nanomaterials, the breakdown of organic dyes in an aqueous solution, such as methylene blue (MB) and methyl orange (MO),

CONTACT Abhijit M ✉ abhijit.geology@gmail.com 📍 Dos in Earth Science, Manasagangothri, University of Mysore, Mysuru.



© 2023 The Author(s). Published by Enviro Research Publishers.

This is an  Open Access article licensed under a Creative Commons license: Attribution 4.0 International (CC-BY).

Doi: <http://dx.doi.org/10.12944/CWE.18.1.18>

is frequently utilized for probe reaction.^{8,9} Because of its benefits, the adsorption process has been effectively used to remove pollutants among a variety of removal approaches.¹⁰

CaSiO₃ is a composition of wollastonite that can be either natural or synthetic. Since the Hench discovery, many biomaterials have become increasingly popular as highly anticipated biomaterials for orthopedic surgery, especially calcium silicate (Wollastonite) and bioactive glass-based materials.^{11,12} Wollastonite is a polymeric material that crystallizes in two different mineral forms, one at low temperatures where it forms a chain silicate, and the other at high temperatures where it forms a triclinic lattice.¹³ Silicon is a crucial trace element that has demonstrated an encouraging role in the premature development of bones. CaSiO₃ has undergone substantial research to be used as dental roots and artificial bones. Since then, CaSiO₃ has become more and more popular in the therapeutic setting, particularly in orthopaedic surgery and drug delivery.^{14,15,16} Generally solid-state and sol-gel methods were previously employed to synthesize the wollastonite, the formation of crystallite can be effectively aided by hydrothermal processes carried out in an autoclave.¹⁷ Solid-state reactions are the most widely utilized of the above practical procedures because they are non-toxic, ecologically acceptable, solvent-free, waste-free synthetic routes unlike other chemical methods, and economical.¹⁸ Numerous efforts have been made to understand the photocatalytic destruction of organic molecules by ZnO.¹⁹ Ideal photocatalysts have tuneable characteristics like band gap reduction for absorption and doping. They also have a large surface area with broad absorption spectra, are inexpensive, and are safe.²⁰ Zinc oxide nanostructure reduces charge recombination and boosts the efficiency of absorption under sunlight.²¹ Considering that morphology actively participates in catalytic actions that affect the separation of the transfer of photogenerated charges, band gap structure.²² In this paperwork, hydrothermal synthesis of fibrous ZnO doped wollastonite was achieved, and the degradation of MB and MO was compared under sunlight. The degradation process can be used at any time and on any sunny day because it is quick, inexpensive, non-toxic, and light-independent.

Materials and Method

Synthesis

Preliminary preparation of Zn-doped wollastonite

The basic preparation was done by magnetic stirrer with two major chemicals Calcium Hydroxide (M.W-74.09 g/mol) + Silicon hydroxide colloidal hydrate (M.W-60.08 g/mol) with suitable stoichiometry placed in a beaker mixed with the 200ml distilled water before preparing this solution calcium hydroxide and Zinc oxide was mixed in different ratios as follows.

- Ca (OH)₂ and ZnO in the percentage of 45% and 5% respectively, this solution was mixed with 50% of SiO₂.
- Ca (OH)₂ and ZnO in the percentage of 40% and 10% respectively, this solution was mixed with 50% of SiO₂.

These two ratios solution was placed in the two separate beakers placed on the magnetic stirrer. The beaker was heated at a temperature of 45°C and stirred in a magnetic stirrer for 3 days aging to mix well and to prepare the precursor. The compound solution was ready to synthesize under hydrothermal conditions.

Hydrothermal Synthesis

The chemicals used for the syntheses are commercial reagent grade used for the modification of fibrous wollastonite rather than other commercial variety crystals. The experiment was carried out with suitable stoichiometry of chemicals at 1050°C temperature and an isobaric condition of 1.01325 bar atmospheric pressure. The compounds were placed in Teflon-lined two different autoclaves to treat under hydrothermal conditions. After aging for reaction time, the compound placed inside the oven was cooled down by quenching with water to arrest the reaction and removed from the autoclaves. The resultant product was dried at 60°C before it was filtered by Whatman filter paper to remove the water content in the samples. The double distilled water was used to wash the product and dried it at room temperature. The resultant product was ready for characterization as 5% Zn-doped wollastonite as Zn-WO-1 and 10% Zn-doped wollastonite as Zn-WO-2.

Characterization

SEM was used to examine the morphology of heated materials. Employing a Rigaku Smart Lab II (Cu K radiation, $\lambda = 1.5414 \text{ \AA}$) X-ray diffract meter and EDAX measurement. A Sorptomatic 1990 instrument's the BET method used for surface area measurements. At liquid nitrogen temperature, measurements of desorption and adsorption were made using nitrogen gas. While BET surface area and pore volume were calculated using conventional software, pore size distribution and volume were examined using the Barrett-Joyner-Halenda (BJH) approach, and the diffuse-reflectance spectra of nanoparticles were measured in the UV-visible wavelength range.

Photocatalytic Degradation Experiments

To analyze the Zn-doped wollastonite photocatalytic activity, MB and MO dyes were employed. This procedure involved mixing of aqueous solution separate 200 ml of MB and MO (10 mg/L) with a produced solution that was then added with 20,

40, 60, and 80 mg of Zn-WO as a photocatalyst treated under darkness for 10, 20, and 30 minutes and continuously stirred to observe absorption. By employing a UV-Visible Spectrophotometer, the photocatalytic property of Zn-wollastonite was lastly examined during various times, such as 30, 60, 90, and 120 minutes under sunlight.

Result and Discussion

XRD

The powder diffraction XRD peaks patterns of Zn-WO-1 and Zn-WO-2 obtained at two different samples, with reference to the JCPDS No: 00-27-0088 reveal that the sample was β -Wollastonite. The mineral shows a triclinic crystal system ($\alpha \neq \beta \neq \gamma \neq 90^\circ$) cell parameters were $a=10.137 \text{ \AA}$, $b=11.092 \text{ \AA}$, $c=7.3249 \text{ \AA}$, Volume of Unit cell= 795.92 \AA^3 . Both samples showed a high degree of crystallinity. Figure 1 shows the peaks of the Zn-WO-1 and Zn-WO-2 sample XRD patterns.

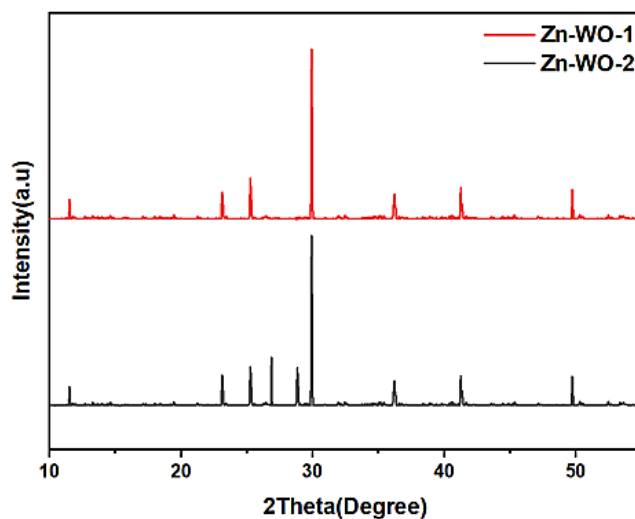


Fig. 1: XRD pattern of Zn-WO-1 and Zn-WO-2 samples.

SEM

A morphology study is the main aim of this paper was conducted through SEM. The Zn-WO-1 and Zn-WO-2 samples are crystallites in a fibrous habit. In figure 2 samples showed crystals are thin wires with a width size of less than $1 \mu\text{m}$. To understand the powdered samples' size and shape, SEM provides topological information. The Zn-WO-2 mineral synthesized shows good fibrous structures when compared with Zn-WO-1.

EDS

The graph of the Zn-WO-1 and Zn-WO-2 samples analysis provides a bulk composition as shown in figure 3 with tables 1 and 2. The percentage of weight for Zn, Ca, Si & O was tabulated. The elemental concentration of stoichiometry composition was used in the experiment and proved by the analysis after the formation of the crystal. In figure 3 we can observe the element identified as most abundant in the samples is oxygen, which has the highest weight

percent of 57.3 in Zn-WO-1 and the lowest weight percent of 54.4 in Zn-WO-2. Si was 18.3 and 16.4 in Zn-WO-1 and Zn-WO-2 respectively. Ca was 19.8 and 19.5 in Zn-WO-1 and Zn-WO-2 respectively. Zn

was an important element and is present in greater amounts in Zn-WO-2 (9.7 weight percent) than in Zn-WO-1 (4.6 weight percent).

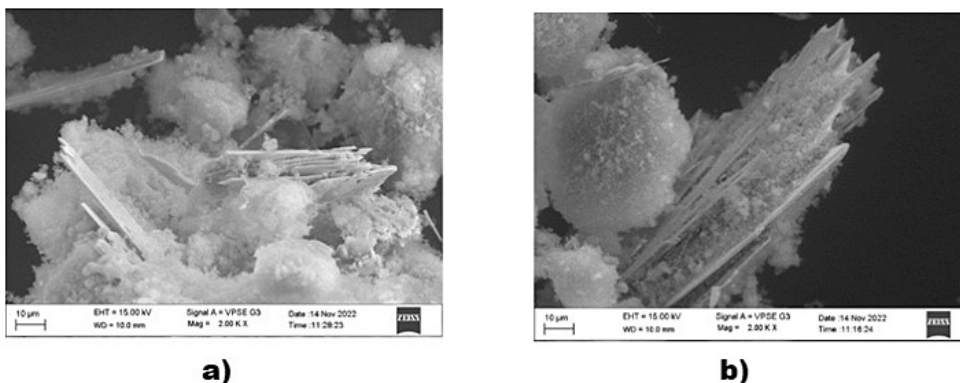


Fig. 2: SEM images of a) Zn-WO-1 and b) Zn-WO-2 samples.

Bet Surface Area Analysis

N₂ adsorption isotherm analysis was used to determine BET surface area. Zn-WO-1 and Zn-WO-2 had excellent BET surface area. Figure 4 shows the N₂ sorption-desorption isotherms of the Wollastonite, according to the IUPAC classification

the material was mesoporous. Although the pore volume and average pore size were calculated by the BJH method.²³ The pore size is quite close to the mesoporous size; thus, it can be regarded as microporous. Data is tabulated in table :3

Element	Weight %	Atomic %
O K	57.3	71.9
Si K	18.3	12.2
Ca K	19.8	14.2
Zn K	4.6	1.7

Table: 1

Element	Weight %	Atomic %
O K	54.4	69.3
Si K	16.4	11.7
Ca K	19.5	14.5
Zn K	9.7	4.5

Table: 2

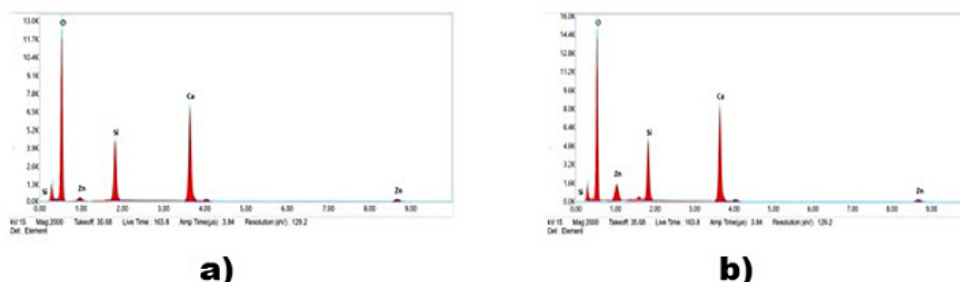


Fig. 3: EDS mapping of a) Zn-WO-1 and b) Zn-WO-2 samples.

Table 3: BET Surface area analysis

Sample Name	Mineral Surface Area (m ² /g)	Pore Volume (cm ³ /g)	Pore Diameter (nm)
Zn-WO-1	92.4	0.112	6.0
Zn-WO-2	112.6	0.132	9.0

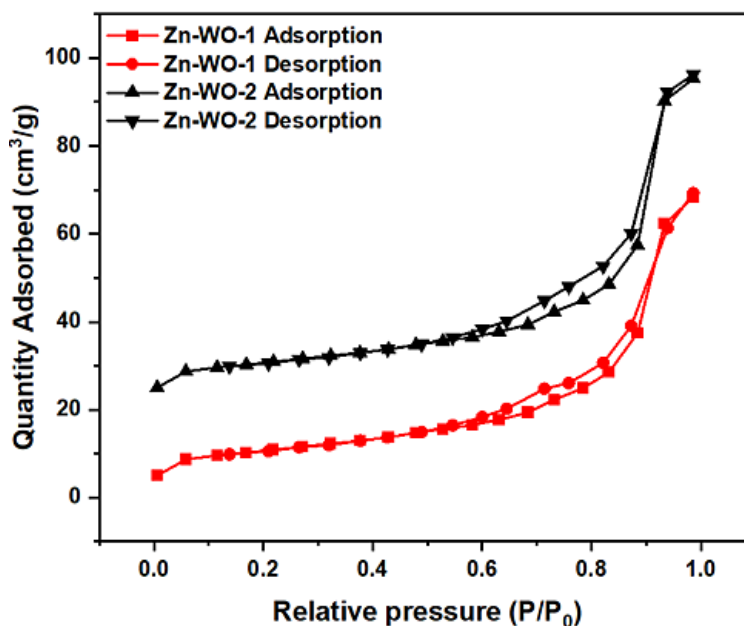


Fig. 4

UV-Vis Studies

Photocatalytic activity is greatly influenced by a photocatalyst's optical quality and energy band structure.²⁴ The Tauc plot for calculating the optical bandgap energies and UV studies of Zn-WO-1 and Zn-WO-2 is shown in figure 5a. In the UV and visible areas, the spectra of all the materials exhibit considerable absorption. While Zn-WO-1 and Zn-WO-2 had a similar absorbance profile with maximum absorption.

$$(\alpha h\nu) = A(h\nu - E_g)^{1/2} \dots(1)$$

Where A is proportional constant, h is the Planck constant, ν frequency, α is the absorption coefficient, and E_g is the bandgap energy. The value of the optical energy bandgap is obtained by extrapolating the Tauc plot graph of $(\alpha h\nu)^2$ against $h\nu$. The band gap as shown in figure 5b values were 2.70 eV and 2.62 eV for Zn-WO-1 and Zn-WO-2 respectively

Photocatalytic Degradation of MB and MO

Zn-WO particles further lowered the content of methylene blue under sunlight before it was treated under darkness. To create an equilibrium between photocatalysts and the dye, the reaction solution was agitated in the dark for 30 minutes. The suspension was then continuously stirred while being exposed to sunshine.²⁵ Using a UV-Visible spectrophotometer, the concentrations of MB and MO were determined at different time intervals and calculated the percentage by equation (2). Zn-WO-1 and Zn-WO-2 were utilized to maintain absorption-desorption equilibrium showing 24.8% and 28.4% of MB, 10.2% and 16.4% of MO dye degradation by absorption under dark. The Zn-WO was a photocatalyst for 120 minutes, Zn-WO-1 and Zn-WO-2 show the concentration of MB dye was degraded up to 88.4% and 92.3% of MO dye was degraded up to 80.9% and 85.3% respectively was plotted in figure 6a.

$$v = (1 - C/Co) * 100 \quad \dots(2)$$

The solution's concentrations before (C_o) and after (C) irradiation with respect to t min, C_o and C are the concentrations of the solution before and

following irradiation for the duration t in minutes, and the kinetic rate constant is K . Both samples are comparable with the pseudo-first-order kinetic model R^2 values for the linear plot of $\ln(C/C_o)$ with a time greater values than 0.9. (Figure 6b).

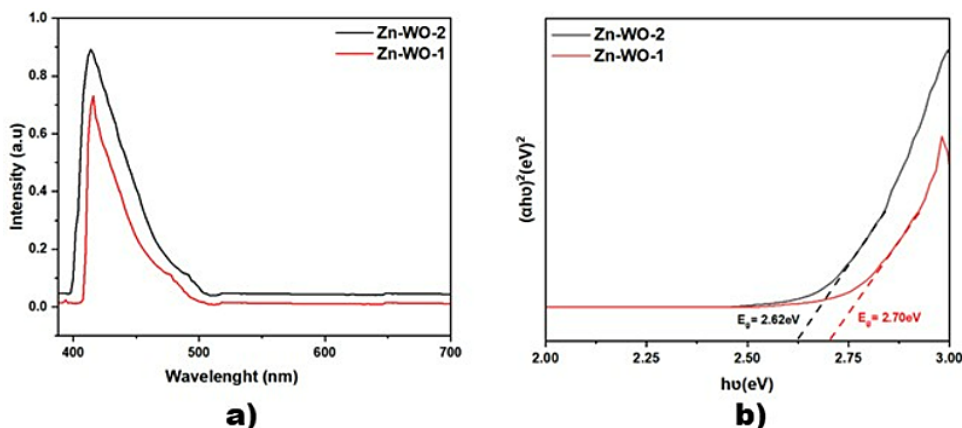


Fig. 5: (a) Uv Studies, (b) Tauc plot of Zn-WO-1 and Zn-WO-2 samples

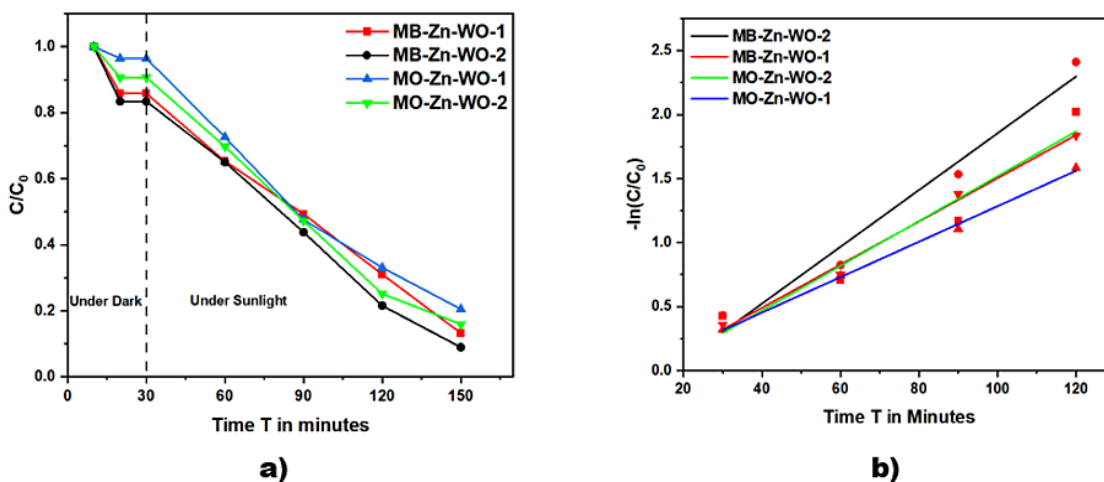


Fig. 6: Degradation of MB and MO. a) Photocatalytic activity. b) The pseudo-first-order kinetic model of Zn-WO-1 and Zn-WO-2 samples

Material Reusability and pH Observation

The study was conducted for Zn-WO-1 and Zn-WO-2 as these nanoparticles have shown good photocatalytic activities under UV light. For the reusability investigation, after each cycle, nanoparticles were separated by centrifugation, dried at 60 °C for an hour, and then used for the following cycle. ZnO in the SiO₂ structure, which facilitates effective electron transfer during

photosynthesis due to various oxidation states increased efficiency for Zn-WO. Even after five cycles of use, nanoparticles maintain good stability and efficiency, virtually matching the performance of photocatalysts studied here shown in figure 7 b. The ph observed here shows maximum degradation occurs at ph 8 further increasing ph reduces the degradation capacity shown in figure 7 a.

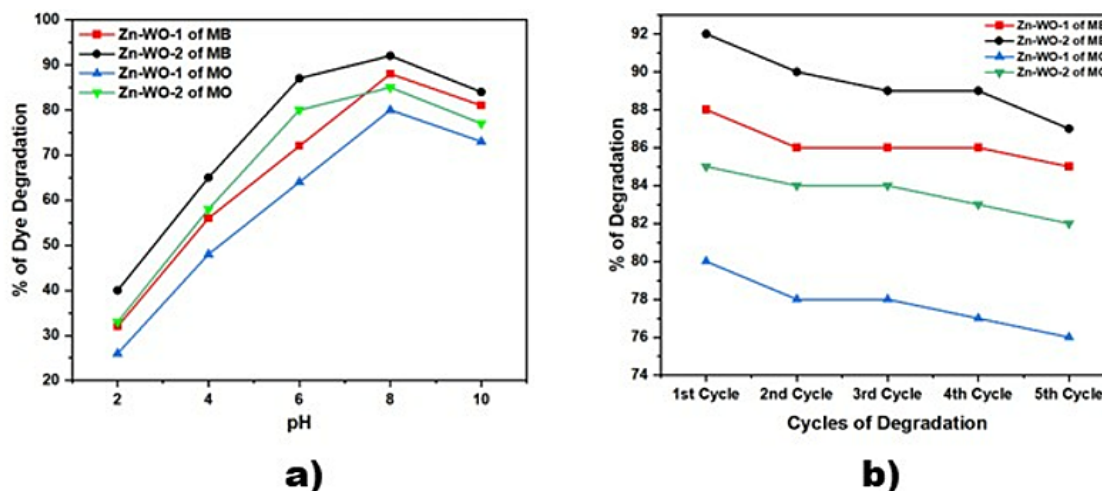


Fig. 7: Degradation of MB and MO. a) pH, b) Degradation Cycles of Zn-WO-1 and Zn-WO-2 sample.

Conclusion

The unique fibrous habit solid-state Zn doped wollastonite composites were successfully synthesized in a simple and inexpensive technique with the isobaric and isothermal conditions. XRD confirmed the production of Zn-WO nanoparticles. SEM analysis of the morphology shows that the sample contains fibrous wollastonite with a rougher surface. The BET method displays a large surface area and excellent pore diameter of 6.0 nm and 9.0 nm for Zn-WO-1 and Zn-WO-2 respectively. The UV-Visible spectrophotometer was used to investigate the optical characteristics. It was discovered that the produced Zn-WO-2 has a smaller band gap than Zn-WO-1. The MB and MO degradation studies demonstrated the Zn-WO nanoparticle's efficiency as a photocatalyst. Additionally, as an active species in the photocatalyst dye degradation of MB and MO dye, $\bullet\text{OH}$ plays a significant role. With an increase in Zn content, composite materials can absorb more

visible light by decreasing the band gap of Zn-WO-2 than Zn-WO-1. When compared to Zn-WO-1, the Zn-WO-2 sample shows the highest photocatalytic performance towards MB and MO under visible light. The sample also exhibits good reusability and stability after five cycles with a slight drop and at pH 8 shows more absorption capacity of nanoparticles.

Acknowledgment

The authors acknowledge that the Vijnana Bhavana is a central instrumentation facility of the University of Mysore. The Institution of Excellence (IOE) for providing characterization facilities.

Funding

There is no funding or financial support for this research work.

Conflict of Interest

No conflict of interest exists.

References

1. Shahid S Shah; Taniya Sharma; Bashir A Dar; Rajinder K. Bamezai, Adsorptive removal of methyl orange dye from aqueous solution using populus leaves: Insights from kinetics, thermodynamics, and computational studies. *Environmental Chemistry and Ecotoxicology*, 2021, Volume 3, 172-181.
2. Yaseen D. A, Scholz M, Textile dye wastewater characteristics and constituents of synthetic effluents: a critical review, *Int. J. Env. Sc. Technol*, 2019, 16, 1193–1226.
3. Oloo C. M, Onyari J. M, Wanyonyi W. C, Wabomba J. N, Muinde V. M, Adsorptive removal of hazardous crystal violet dye from aqueous solution using *Rhizophora mucronata* stem-barks: equilibrium and kinetics studies, *Environ. Chem. Ecotoxicol*, 2020, 2, 64–72.

4. Haitham K, Razak S, Nawi M. A, Kinetics and isotherm studies of methyl orange adsorption by a highly recyclable immobilized polyaniline on a glass plate, *Arab. J. Chem*, 2019, 12 (7), 1595–1606.
5. Vucurovic V. M, Razmovski R. N, Miljic U. D, Puskas V. S, Removal of cationic and anionic dyes from aqueous solutions by adsorption on maize stem tissue, *J. Taiwan Inst. Chem. Eng.*, 2014, 45 (4), 1700–1708.
6. Huang M, Yu J, Li B, Deng C, Wang L, Wu W, Dong L, Zhang F, Fan M, Intergrowth and coexistence effects of TiO₂–SnO₂ nanocomposite with excellent photocatalytic activity, *J. Alloy. Compd.*, 2015, 55, 629.
7. Wang C, Shao C, Zhang X, Liu Y, SnO₂ Nanostructures-TiO₂ Nanofibers Heterostructures: Controlled Fabrication and High Photocatalytic Properties, *Inorg. Chem.*, 2019, 48, 7261.
8. Hosseinpour-Mashkani S. M, Sobhani-Nasab A, Investigation of photovoltaic properties of silver-doped ZnTiO₃ nanoparticles, *J. Mater. Sci.*, 2017, 28, 4345.
9. Salavati-Niasari M, Soofivand F, Sobhani-Nasab A, Shak-ouri-Arani M, Yeganeh Faal A, Bagheri S, Synthesis, characterization, and morphological control of ZnTiO₃ nanoparticles through sol-gel processes and its photocatalyst application, *Adv. Powder Technol.*, 2016, 27, 2066.
10. Xiaoliang Liang; Sanyuan Zhu; Yuanhong Zhong; Jianxi Zhu; Peng Yuan; Hongping He; Jing Zhang. The remarkable effect of vanadium doping on the adsorption and catalytic activity of magnetite in the decolorization of methylene blue, *Applied Catalysis B: Environmental*, 2010, 97, 151–159.
11. Huebner J. S, *Rock-Forming Minerals: Single-chain Silicates*, Volume 2A, second ed, Geological Society of London, 1997, 1997, *J. Geol.* 90 (1982) 748–749.
12. Li X, Shi J, Zhu Y, Shen W, Li H, Liang J, Gao J, A template route to the preparation of mesoporous amorphous calcium silicate with high in vitro bone-forming bioactivity. *Journal of Biomedical Materials Research Part B: Applied Biomaterials*, 2007, 83(2), 431-439.
13. Palakurthy, Srinath, Venu Gopal Reddy K, Samudrala, Raj Kumar, Abdul Azeem P, In vitro bioactivity and degradation behavior of β -wollastonite derived from natural waste. *Materials Science and Engineering: C*, 2019, 98(1), 109–117.
14. Ding S. J, Shie M. Y, Wang C. Y, Novel fast-setting calcium silicate bone cements with high bioactivity and enhanced osteogenesis *in vitro*. *Journal of Materials Chemistry*, 2009, 19(8), 1183- 1190.
15. Taddei P, Tinti A, Gandolfi M. G, Rossi P. L, Prati C, Ageing of calcium silicate cements for endodontic use in simulated body fluids: a micro-Raman study. *Journal of Raman Spectroscopy*, 2009, 40(12), 1858-1866.
16. Wu J, Y.-J. Zhu, F. Chen, X.-Y. Zhao, J. Zhao, C. Qi, Amorphous calcium silicate hydrate/block copolymer hybrid nanoparticles: synthesis and application as drug carriers. *Dalton Transactions*, 2013, 42(19), 7032-7040.
17. K. Lin, Chang J, Lu J, Synthesis of wollastonite nanowires via hydrothermal microemulsion methods, *Mater. Lett.*, 2006, vol. 60, no. 24, pp. 3007– 3010.
18. Lusi Ernawati, Ruri Agung Wahyuono, Andromeda Dwi Laksono, Andriati Ningrum, Kurnia Handayani, Audi Sabrina, Wollastonite (CaSiO₃)-based Composite Particles for Synthetic Food Dyes (Brilliant Blue) Removal in Aquatic Media: Synthesis, Characterization and Kinetic study. *IOP Conference Series: Materials Science and Engineering*, *Mater. Sci. Eng*, 2021, 1053 012001.
19. Kouser S, Hezam A, Byrappa K, and Khanum S. A, Sunlight-assisted synthesis of cerium (IV) oxide nanostructure with enhanced photocatalytic activity, *Optik (Stuttg.)*, 2021, vol. 245, p. 167236.
20. Dafeng Zhang, Yunxiang Tang, Xiaoxue Qiu, Jie Yin, Changhua Su, and Xipeng Pu. Use of synergistic effects of the co-catalyst, pn heterojunction, and porous structure for improvement of visible-light photocatalytic h₂ evolution in porous ni₂o₃/mn_{0.2}cd_{0.8}/cu₃p@ cu₂s. *Journal of Alloys and Compounds*, 2020, 845:155569.
21. Chuansheng Chen, Wei Mei, Chen Wang, Zhi Yang, Xian Chen, Xiaohua Chen, and Tianguai Liu. Synthesis of a flower-like sno/zno nanostructure with high catalytic activity

- and stability under natural sunlight. *Journal of Alloys and Compounds*, 2020, 826:154122.
22. Zhenghua Fan, Fanming Meng, Jinfeng Gong, Huijie Li, Youdi Hu, and Daorui Liu. Enhanced photocatalytic activity of hierarchical flower-like $\text{CeO}_2/\text{TiO}_2$ heterostructures. *Materials Letters*, 2016 175:36–39.
23. Samskruthi K. P, Ananda S, Nandaprakash M. B, and Chandrakantha K. S, Synthesis and Characterization of SnO_2 and SnO_2/ZnO Nanoparticles by Electrochemical Method: Evaluation of their Performance in Photodegradation of Indigo Carmine Dye and Antibacterial Activity, *Asian J. Chem*, 2020, vol. 32, no. 9, pp. 2119–2124.
24. Akbar Eslami, Simin Nasser, Bahram Yadollahi, Alireza Mesdaghinia, Foroogh Vaezi, Ramin Nabizadeh, Shahrokh Nazmara, Photocatalytic degradation of methyl tert-butyl ether (MTBE) in contaminated water by ZnO nanoparticles. *Journal Chemical and Technology Biotechnology*, 2008, 83: 1447-1453.
25. Alkanad K, Ali O, Hezam S. S. G. C. A, Abdullah Bajiri M, and L. N. K., “ Highly Efficient Degradation of Organic Compounds via $\beta\text{-Bi}_2\text{O}_3$ Semiconductor Under Visible Illumination,” *IOP Conf. Ser. Mater. Sci. Eng*, 2022, vol. 1221, no. 1, p. 012040.